Indoor Air 2014; 24: 93–102
wileyonlinelibrary.com/journal/ina
Printed in Singapore. All rights reserved

INDOOR AIR
doi:10.1111/ina.12050

Nonlinear eddy viscosity modeling and experimental study of jet spreading rates

Abstract Indoor airflow pattern is strongly influenced by turbulent shear and turbulent normal stresses that are responsible for entrainment effects and turbulence-driven secondary motion. Therefore, an accurate prediction of room airflows requires reliable modeling of these turbulent quantities. The most widely used turbulence models include RANS-based models that provide quick solutions but are known to fail in turbulent free shear and wall-affected flows. In order to cope with this deficiency, this study presents a nonlinear k-ε turbulence model and evaluates it along with linear k-ε models for an indoor isothermal linear diffuser jet flow measured in two model rooms using PIV. The results show that the flow contains a free jet near the inlet region and a wall-affected region downstream where the jet is pushed toward the ceiling by entrainment through the well-known Coanda effect. The CFD results show that an accurate prediction of the entrainment process is very important and that the nonlinear eddy viscosity model is able to predict the turbulence-driven secondary motions. Furthermore, turbulence models that are calibrated for high Reynolds free shear layer flows were not able to reproduce the measured velocity distributions, and it is suggested that the model constants of turbulence models should be adjusted before they are used for room airflow simulations.

C. Heschl[1], K. Inthavong[2], W. Sanz[3], J. Tu[2]

[1]Fachhochschule Burgenland, University of Applied Science, Pinkafeld, Austria, [2]Platform Technologies Research Institute, School of Aerospace, Mechanical and Manufacturing Engineering, RMIT University, Bundoora, Victoria, Australia, [3]Institute for Thermal Turbomachinery and Machine Dynamics, Graz University of Technology, Graz, Austria

Key words: Linear diffuser; Jet flow; Turbulent models; Reynolds Averaged Navier Stokes equations; Nonlinear RANS; Spreading rate.

Prof. J. Tu
School of Aerospace, Mechanical and Manufacturing Engineering
RMIT University, PO Box 71, Plenty Road, Bundoora
Victoria 3083, Australia
e-mail: jiyuan.tu@rmit.edu.au

Received for review 18 November 2012. Accepted for publication 8 May 2013.

Practical Implications

A nonlinear version of the standard k-e turbulence model is proposed to improve its performance for the jet spreading found in linear diffusers. The model is evaluated against new measured PIV experimental data that serve as a benchmark for future evaluations of turbulence modeling in indoor airflows. The PIV measurements provide insight into the flow behavior from linear diffusers. The results will help users choose the appropriate default turbulence models that are readily available in commercial CFD software, to suit the indoor air simulation.

Introduction

Indoor airflows subjected to linear jet diffusers feature a rich variety of fluid dynamics. These flow characteristics also exert significant influence on the distribution of contaminant particles suspended in the air, and therefore, the accurate prediction of such airflows plays an important role in the design process of ventilation systems for both occupant comfort and contaminant removal (Chang et al., 2006; He et al., 2005; Inthavong et al., 2012). Computational fluid dynamics (CFD) is a promising tool to capture such flow phenomena. Due to the lower computational effort, most airflow simulations are based on the Reynolds Averaged Navier Stokes equations (RANS) with a first-order-closure turbulence model. While its use has been prominent in recent years as reviewed by Chen and Zhai (2004) and Zhai et al. (2007), the accuracy and reliability of the simulation significantly depend on the implementation of the turbulence model to account for the flow behavior.

Early numerical investigations of two-dimensional room airflows (Nielsen, 1990; Sørensen and Nielsen, 2003; Voigt, 2002) showed that isotropic turbulence models (e.g., a linear eddy viscosity model) were sufficient in predicting the room airflows. However, the standard Boussinesq approach used relies on a linear correlation between the Reynolds stress tensor and the strain rate tensor, which is not able to reproduce the turbulent normal stresses sufficiently. For this reason,

this approach fails in the prediction of turbulence-driven secondary motions (Demuren and Rodi, 1984; Heschl et al., 2013; van Hooff et al., 2013). For room airflows, this scenario can be observed at air diffusers or inlets that are mounted near a wall so that a three-dimensional wall jet is encountered. The large lateral to normal spreading rates caused by the redistribution of the turbulent normal stresses near the wall are not captured by linear correlation turbulence models, leading to poor predictions in downstream flow (Abrahamsson, 1997; Craft and Launder, 2001; Lübcke & Th. Rung, 2003). A further difficulty in CFD modeling of indoor airflows is the low inlet velocities that produce Reynolds numbers in the range of $\mathrm{Re} \approx 10^2 - 10^4$. In this range, transitional effects influence the entrainment of the inlet jet. Studies have shown that the jet spreading rate is dependent on the Re number (Deo et al., 2007). The importance of the turbulent normal stresses and the transitional effects indicates that a nonlinear eddy viscosity turbulence model (EVM) calibrated with regard to normal stresses and flow entrainment is indispensable for an accurate prediction of room airflows.

Therefore, the purpose of this study is the development of a nonlinear eddy viscosity model capable to simulate the room flow phenomena described previously. Starting from the investigation of the performance of k-ε turbulence models in the prediction of the lateral spreading rate of isothermal three-dimensional wall jets, a nonlinear eddy viscosity modification is made to the standard k-ε model and its model constants are calibrated based on experimental data (isothermal case). For this reason, two model rooms with different widths and heights and a linear diffuser inlet producing a wall jet flow across the ceiling are investigated experimentally using particle image velocimetry (PIV) and used to evaluate the k-ε turbulence models.

Experimental setup

The test setup consists of an air supply duct system, a model room made of plexiglass in an air-conditioned test room and a PIV measurement system (Figure 1). The test rig is equipped with a frequency-controlled fan unit, which feeds the air via an orifice plate, a rectifier, a mass flow measurement unit, temperature sensors, and seeding mixing chamber to the plexiglass test model. The plexiglass model is placed inside a black-coated test room to allow optimum illumination, while thermal influences are minimized by placing the laser energy supply and the computer equipment outside of the test room. During the measurements, temperatures of the inlet, outlet, and surrounding walls, the relative humidity, and the ambient pressure are logged, so that the air properties can be determined to ensure an isothermal case.

Plexiglass models

The two plexiglass model rooms with their dimensions are shown in Figure 2. They differ in their length-to-height and length-to-width ratios and in their outlets. Both models have an inlet air supply duct with evenly distributed holes. The supply ducts are fed from both end sides over a flow rectifier. For Room-1, the air supply extends over a length of 666 mm and contains 222 holes (2-mm diameter) evenly spaced along the duct. The mean inlet velocity is 14.84 m/s (air change rate ACH = 84), and the inlet angle is 16° downwards from the horizontal direction. The air leaves the model room through a small channel of 12 mm height and the same length of 666 mm at the opposite wall of the room. Additional parameters are as follows: H = 400 mm, D/H = 0.001, W/H = 2.0, L/H = 3.0.

The air supply of the second model room contains seven groups of 32 holes with a diameter of 1.3 mm over an overall length of 440.8 mm. The distance between the holes is 1.5 mm and between the seven-hole groups 13.5 mm. The mean inlet velocity is 36.88 m/s (ACH = 84), and the inlet angle is 27.5° downwards from the horizontal direction. The outlet is a duct at the opposite wall which has the same hole distribution as the inlet air supply duct.

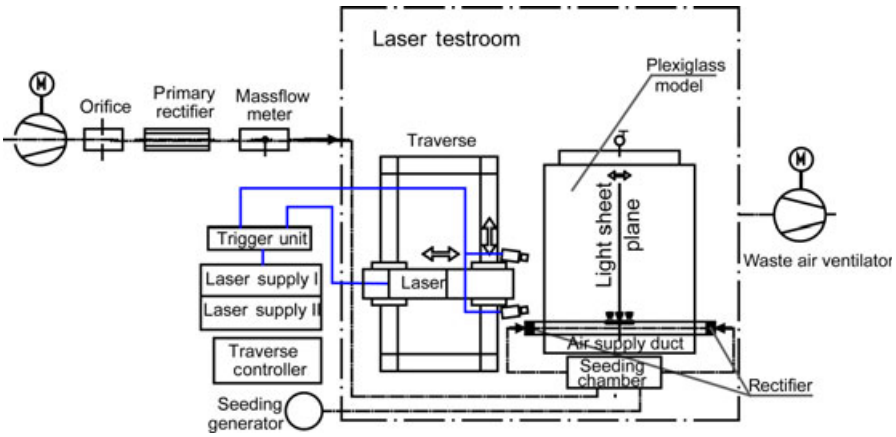

Fig. 1 Schematic of experimental setup for the room flow investigation

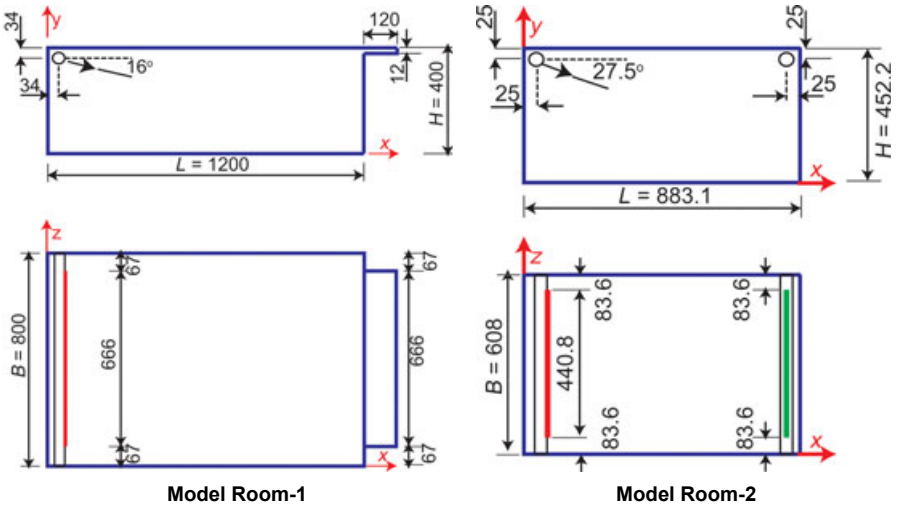

(a) Schematic of the two plexiglass model rooms

Fig. 2 Geometry of the plexiglass model rooms. Dimensions are in mm

PIV measurement setup

The light sheet optic and the two cameras are mounted on a two-dimensional traverse system so that only one calibration is needed for all PIV measurements. The two cameras are mounted on top of each other so that the complete height of the model room can be covered. The field of view of one camera is 155 × 200 mm², so that in x-direction 294, in y-direction 110, and in z-directions 39 measured positions were obtained. This yields in a measured domain ranging from $x = 110$ to 1200 mm, $y = 0$ to 400 mm, and $z = 0$ to 800 mm which consists of about 1,300,000 vectors. To eliminate the turbulent fluctuations, the measuring data are averaged over a measuring period of 30 s with a sample rate of 4 Hz.

The field of view of one camera was 155 × 200 mm², so that the complete height of the model room could be measured at the same time for every position. For all PIV measurements, two cameras with a resolution of 1344 × 1024 pixels are used. The interrogation areas are defined with 32 × 32 pixels and an overlapping of 25%. In the z-direction, the light sheet probe and cameras were traversed in steps of 20 mm to determine the x and y velocity components in about 40 measurements planes normal to the z-axis.

Measurement uncertainty analysis was performed following Coleman & Steele (1995). The accuracy of velocity measurement is limited by the accuracy of the sub-pixel interpolation of the displacement correlation peak. In this study, the cross-correlation is performed using the adaptive correlation method (Dantec, 2002). Based on the size of the interrogation area, the adaptive correlation is used to calculate the instantaneous vector maps, and the large number of instantaneous vector maps is used to calculate the mean velocity. For our data, this leads to an uncertainty in the streamwise and wall-normal mean velocities at 95% confidence level of ±2.3% and ±2.9%, respectively.

Numerical method

In the CFD model, the inlet consisting of individual holes was simplified to a single slot with the hole diameter as its height. Due to the larger inlet area, the inlet velocity was reduced to achieve the same mass flow. To obtain the same momentum, a small volume in the inlet area of the slot was created where a momentum source was defined to match the original supply duct. This technique is known as the *momentum method* (Srebric and Chen, 2002). Preliminary CFD simulations were performed and compared with the PIV measurements, prior to performing the full room simulations.

The steady-state continuity and momentum RANS equations for incompressible fluids and isothermal flow are as follows:

$$\frac{\partial u_j}{\partial x_j} = 0 \tag{1}$$

$$\bar{u}_j \frac{\partial u_i}{\partial x_j} = -\frac{1}{\rho}\frac{\partial p}{\partial x_i} + \frac{\partial}{\partial x_j}\left[\nu \frac{\partial u_i}{\partial x_j}\right] - \frac{\partial \overline{u_i' u_j'}}{\partial x_j} \tag{2}$$

To close the equation system, the Reynolds stresses $-\rho u_i' u_j'$ must be modeled. Typically, this is achieved by the linear eddy viscosity concept, where the turbulent stress tensor is expressed by a linear correlation between the strain rate tensor S_{ij} and the Reynolds stress tensor

$$-\rho \overline{u_i' u_j'} = \rho C_\mu L_t U_t S_{ij} - \frac{2}{3}\rho k \delta_{ij} \tag{3}$$

where C_μ is a model constant, U_t and L_t are turbulent velocity and length scales, respectively, and k is the turbulence kinetic energy.

Standard *k*-ε turbulence model and its modifications

To close the linear eddy viscosity turbulence model, the turbulent velocity scale and the turbulent length or time scale must be determined. For the standard *k*-ε turbulence model, two additional transport equations for the turbulence kinetic energy k and the rate of dissipation ε are used to achieve this. The equations are given as

$$\rho u_j \frac{\partial k}{\partial x_j} = \frac{\partial}{\partial x_i}\left[\left(\mu + \frac{\mu_t}{\sigma_k}\right)\frac{\partial k}{\partial x_i}\right] + P_k - \rho\varepsilon \tag{4}$$

$$\rho u_j \frac{\partial \varepsilon}{\partial x_j} = \frac{\partial}{\partial x_i}\left[\left(\mu + \frac{\mu_t}{\sigma_\varepsilon}\right)\frac{\partial \varepsilon}{\partial x_i}\right] + \frac{C_{\varepsilon 1} P_k - C_{\varepsilon 2}\rho\varepsilon}{T} \tag{5}$$

The time scale, $T = \frac{L_t}{U_t}$, and the velocity scale are determined by $T = k/\varepsilon$ and $U_t = \sqrt{k}$, respectively, and the turbulent viscosity is expressed as

$$\mu_t = \rho C_\mu \frac{k^2}{\varepsilon}. \tag{6}$$

The standard empirical model constants are $C_\mu = 0.09$, $C_{\varepsilon 1} = 1.44$, and $C_{\varepsilon 2} = 1.92$.

The standard *k*-ε model is a semi-empirical model derived primarily for high Reynolds number flows and thus valid for flow regions far from wall boundaries (turbulent core flow). For low Reynolds number flows, such as those found near walls, wall functions (Launder and Spalding, 1974) are typically used to connect the turbulent core flow with the near-wall flow. In this study, an enhanced wall function is used which implies a fine near-wall mesh where the first node from the wall is placed around $y^+ = 1$, to resolve the viscous sublayer. Modifications to improve the standard *k*-ε (SKE) model include the Realizable *k*-ε model (RKE) by Shih et al. (1995) and the Renormalization Group *k*-ε model (RNG) by Yakhot and Orszag (1986).

Nonlinear *k*-ε turbulence model

Nonlinear turbulence models include nonlinear terms of the strain rate for the definition of the Reynolds stresses, so that the Reynolds stresses can be based on the Reynolds stress anisotropy tensor b_{ij} as

$$b_{ij} = \frac{\overline{u_i' u_j'}}{2k} - \frac{1}{3}\delta_{ij}. \tag{7}$$

In principle nonlinear eddy viscosity, models assume that the anisotropy tensor depends on the local velocity gradients, vorticity, and the turbulent time scale which can be summarized in the following form:

$$b_{ij} = \sum_\lambda G_\lambda T_{ij}^\lambda \qquad T_{ij} = T_{ij}\left(S_{ij}, \Omega_{ij}, T_t\right) \tag{8}$$

where

$$S_{ij} = \left(\frac{\partial u_i}{\partial x_j} + \frac{\partial u_j}{\partial x_i}\right) \qquad \Omega_{ij} = \left(\frac{\partial u_i}{\partial x_j} - \frac{\partial u_j}{\partial x_i}\right) \tag{9}$$

where G_λ are model constants, T_{ij} is a nonlinear function of the local velocity gradients expressed by the shear rate tensor S_{ij} and the vorticity tensor $\mathbf{\Omega}_{ij,}$ and T_t is the turbulent time scale; for a nonlinear *k*-ε model, $T_t = k/\varepsilon$. For the modeling of the Reynolds stress anisotropy tensor $b_{ij,}$ the approach of Gatski and Speziale (1992) is used, where

$$b_{ij} = G_1 T_t S_{ij} + G_2 T_t^2\left(S_{ik}S_{kj} - \frac{1}{3}S_{kl}S_{kl}\delta_{ij}\right) + G_3 T_t^2\left(\Omega_{ik}S_{kj} - \Omega_{jk}S_{ki}\right). \tag{10}$$

With the model constants

$$G_1 = -C_\mu, G_2 = -C_1, G_3 = -C_2. \tag{10}$$

For calibration of the model constants C_1 and $C_{2,}$ existing experimental and DNS data from simple shear flows are used [Kim et al. (1987), Tavoularis and Karnik (1989), Tavoularis and Corrsin (1981), De Souza et al. (1995)] and plotted in Figure 3 as these flows correspond well to jet flows. The dimensionless invariants η and ξ are used to characterize the flow parameters and are defined as:

$$\eta = T\sqrt{2\,S_{ij}S_{ij}} \qquad \xi = T\sqrt{2\,\Omega_{ij}\Omega_{ij}} \tag{11}$$

For homogeneous shear and boundary layer flows, the anisotropy coefficient b_{12} is proportional to η and ξ, and the anisotropy coefficient b_{ii} to η^2 and ξ^2. It is noted that only the values for b_{11} and b_{22} are shown because for simple shear flows, the terms $\left(S_{ik}S_{kj} - \frac{1}{3}S_{kl}S_{kl}\delta_{ij}\right)$ and $\left(\Omega_{ik}S_{kj} - \Omega_{jk}S_{ki}\right)$ in Equation 10 are close to zero for $i = 1$ and $j = 2$. This makes b_{12} mainly dependent on C_μ, (i.e., the influence of C_1 and C_2 becomes negligi-

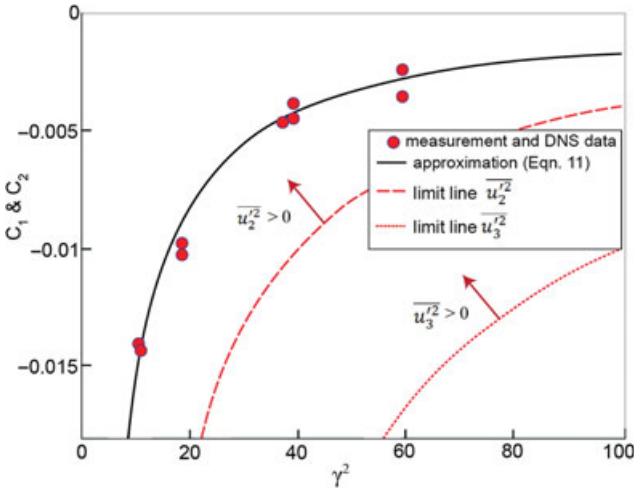

Fig. 3 Dependence of the model constants C_1 and C_2 on the dimensionless parameter γ

ble). A dimensionless invariant γ is introduced to determine the model constants C_1 and C_2, and is defined as

$$C_i = C_i(\gamma^2) \qquad \gamma = \sqrt{0.5\left(\eta^2 + \xi^2\right)}. \tag{12}$$

The dependence of the model constants C_1 and C_2 on the dimensionless invariant γ is shown in Figure 3 where the data points are DNS and experimental data found in literature cited previously. The solid black line represents the corresponding approximation equation found as

$$C_1 = C_2 = \frac{-0.171}{0.9 + \gamma^2}. \tag{13}$$

The dashed lines in Figure 3 show the limits for simple shear stress flows (homogeneous shear flows, two-dimensional channel flow, boundary layer flows etc.), where the turbulent normal stresses $u_2'^2 > 0$ and $u_3'^2 > 0$ are positive. The comparison between the approximation in Equation 13 and the limit lines shows that the proposed nonlinear model always predicts positive turbulent normal stresses, so that a robust and stable numerical solution can be expected.

The computations were performed with the commercial CFD code ANSYS Fluent (Fluent, 2007). The SIMPLE-based segregated solver is used; for the convective terms, the second order upwind discretization is applied. Beside the included turbulence models (SKE, RKE, RNG), the proposed nonlinear eddy viscosity modification was imposed to the SKE model leading to the SKE-NL (nonlinear) model. The implementation into Fluent was performed through UDF (user-defined function) routines where the simulation time of the nonlinear model is 1.3-times longer than with the default models. For both model rooms, a structured mesh with high resolution in the near wall to satisfy the requirements for low-Re turbulence models, that is, y^+ of first grid point <1, was used consisting of 3.5 million cells for Room-1 and 2.5 million for Room-2. The turbulence properties defined at the inlet boundary to define the supply jet were chosen in such a way so that the flow profiles in the near inlet region obtained from the experimental data were matched. For Room-1, a turbulence intensity of 40%, corresponding to a turbulent kinetic energy of 11.2 m^2/s^2, and a dissipation of 42152 m^2/s^3 was used, while for Room-2, the turbulence intensity was 20%, corresponding to a turbulent kinetic energy of 20 m^2/s^2, and the dissipation was 162264 m^2/s^3.

Results and discussion

Nonlinear EVM calibration

Any individual tuning of model constants should be consistent to the log-law layer (Wilcox, 2006). A simple option is to adapt the proportionality factor of the production and dissipation term in the ε equation in such a way that both the measured spreading rate and the logarithmic wall law are fulfilled. For the k-ε-based turbulence models, it is shown in (Pope, 2000) that the following relations for the model parameters are constrained by

$$\kappa^2 = (C_{\varepsilon 2} - C_{\varepsilon 1})\sigma_\varepsilon \sqrt{C_\mu} \tag{14}$$

where κ (kappa) is the von Karman constant. If the spreading rate is known, a specific calibration of the model constants based on the Equations 14 can be achieved. The measurement data obtained in this study provide the mean inlet velocity and the specific jet spreading rate for the two room flows.

For the air supply duct of Room-1, a constant spreading rate of $dy_{1/2}/dx = 0.110$ and of Room-2 of $dy_{1/2}/dx = 0.108$ was determined. The proposed calibration procedure yields $C_{\varepsilon 1} = 1.42$, $\sigma_\varepsilon = 1.23$ for the SKE-NL. The other model constants comply with their default values.

Velocity distribution

A comparison of the measured and predicted velocity distribution is shown in Figure 4 for Room-1 and in Figure 5 for Room-2. In both cases, the flow is characterized by a free jet at the inlet region and a wall-affected region downstream. The latter region is driven by the Coanda effect that pushes the jet toward the ceiling. The measurement of Room-1 exhibits a near symmetric flow, whereas the airflow in Room-2 is asymmetric. This asymmetry may be caused by the smaller room size and its confinement effect which influences the rate of entrainment of ambient air into the jet. For Room-1, the flow behavior is reproduced by all turbulence models except for the RKE model which partly predicts an asymmetric airflow. The RKE model overpredicts the dissipative turbulence interaction so that the entrainment is significantly underpredicted (the measured spreading rate in the inlet area is about $dy_{1/2}/dx = 0.11$ while the RKE predicts ($dy_{1/2}/dx = 0.09$). This leads to a lower entrainment in the shear layer flow and consequently a smaller jet profile with a higher centerline velocity. This behavior of the RKE model can also be observed in Room-2. It underpredicts the entrainment so that a complete attachment of the jet to the wall is suppressed. In contrast, the standard model SKE with a computed spreading rate of $dy_{1/2}/dx = 0.11$ predicts the flow pattern and the velocity distribution clearly better than the RKE and also RNG model. The computed flow pattern indicates that an accurate prediction of the entrainment process is very important. Because of the low inlet velocity, a transitional flow behavior which leads to a high entrainment effect can be expected. Consequently, linear turbulence models that are calibrated for high Reynolds free shear layer flows are not able to reproduce

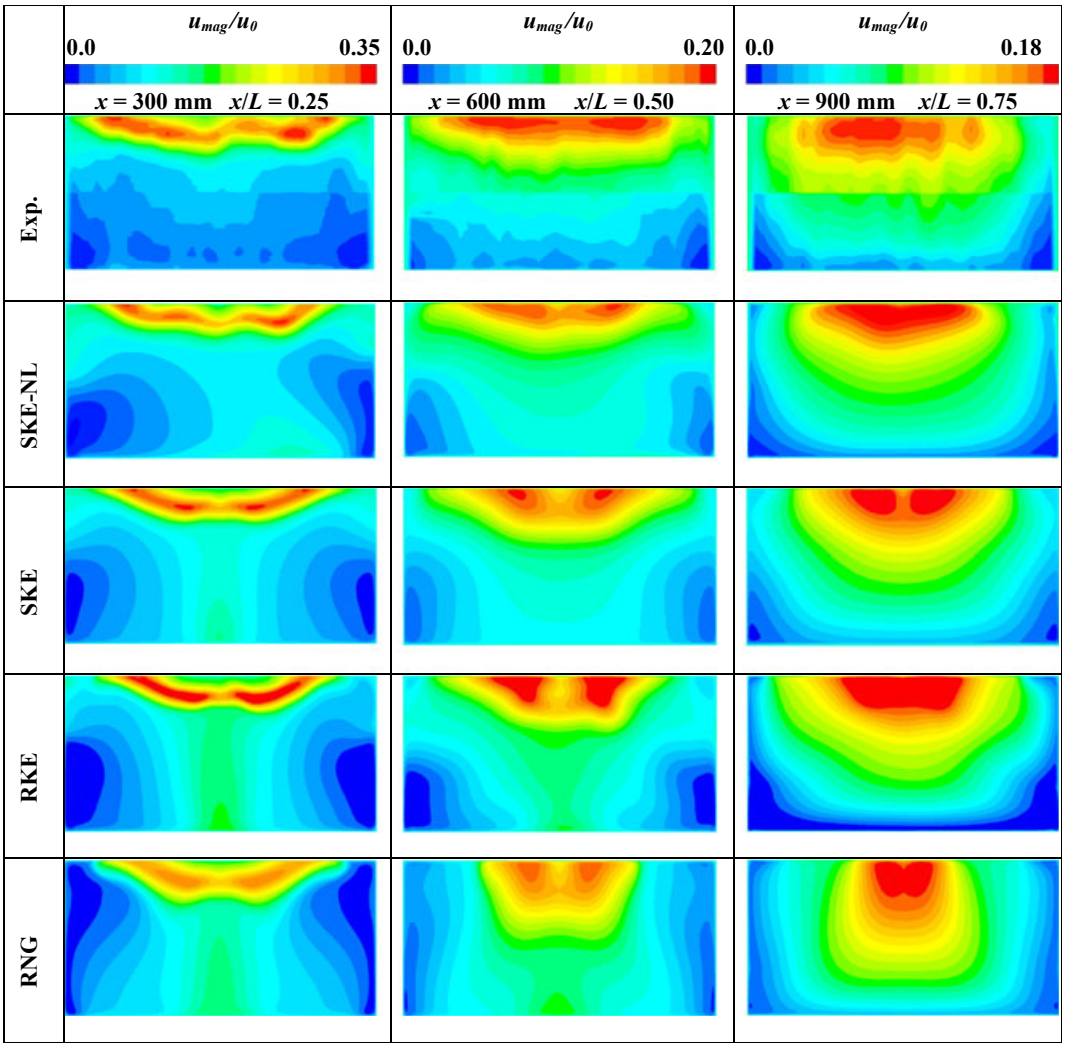

Fig. 4 Comparison of velocity contours in three planes normal to the x-axis in Room-1. The diagrams show the complete cross-section

the observed velocity distribution, and therefore, its model constants should be adjusted before they are used for room airflow simulations.

The effect of the nonlinear modifications considering the influence of the anisotropy based on strain rate and rotation rate can be seen in the velocity contours. The comparison of the velocity distribution for Room-1 (Figure 4) between the SKE and the SKE-NL model shows that the nonlinear model provides better agreement with the experimental findings; particularly, further downstream at $x/L = 0.75$, where the turbulence effects are more distinct and are evident through the wall jet attaching to the ceiling, the flow is more realistically reproduced by the SKE-NL model. Interestingly, the influence of the turbulent normal stresses is not noticeable in Room-2. This may be due to the larger inlet angle so that a hardly visible wall jet arises.

Jet development downstream

The development of the wall jet as it progresses downstream is visualized through a contour plot of the streamwise u-velocity component for both rooms (Figures 6 and 7). The experimental results show a large core region dominated by the jet in the upper half of the room with a positive axial velocity. For Room-1, all turbulence models predict the qualitative jet development fairly well, although the SKE-NL model produces a thinner high velocity region downstream. The development of the wall jet in Room-2 shows a greater jet plume created by the increased inlet angle of the jet. The flow is entrained rapidly and the jet reattaches to the ceiling at approximately $x = 200$ mm. The SKE and RKE model predictions show the jet velocity decaying rapidly, and at $x = 900$ mm, the influence of the jet is diminished.

Velocity profiles for Room-1

Additional quantitative analyses are performed for Room-1 because the flow pattern shows some symmetry, and therefore, values at specific locations should provide a good reflection of the flow characteristics. The u-velocity along the room height at mid-section is

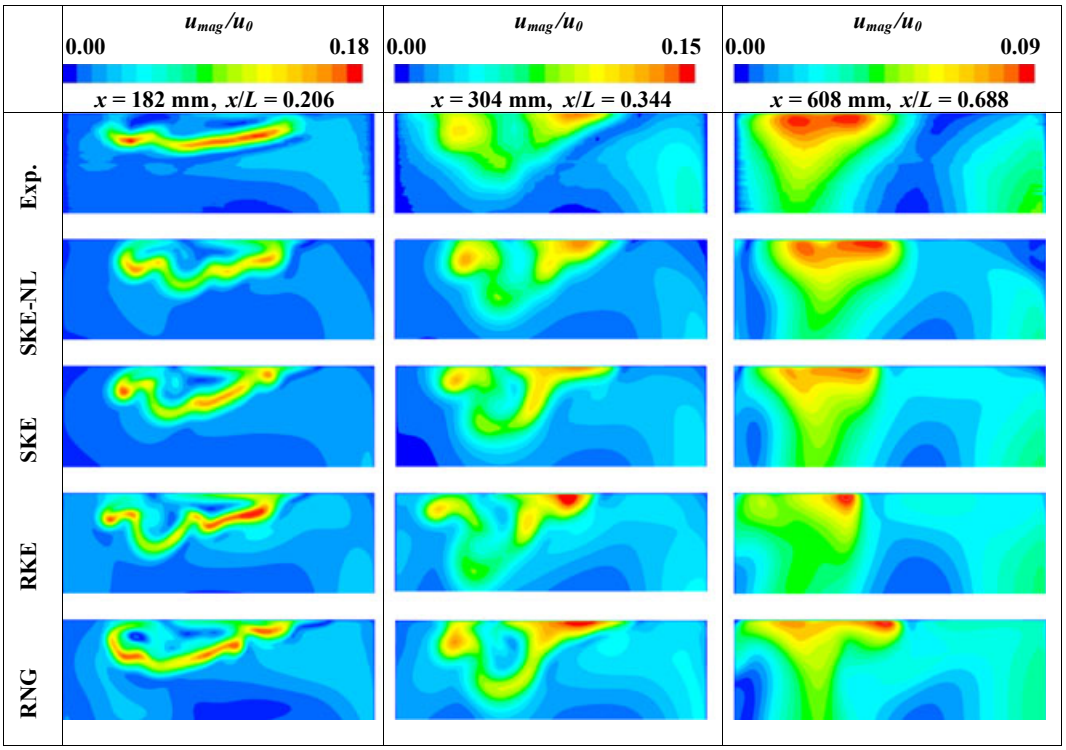

Fig. 5 Comparison of velocity contours in three planes normal to the x-axis in Room-2. Measurement region is a height of 195 mm (from ceiling) and a width of 608 mm (full width of the room)

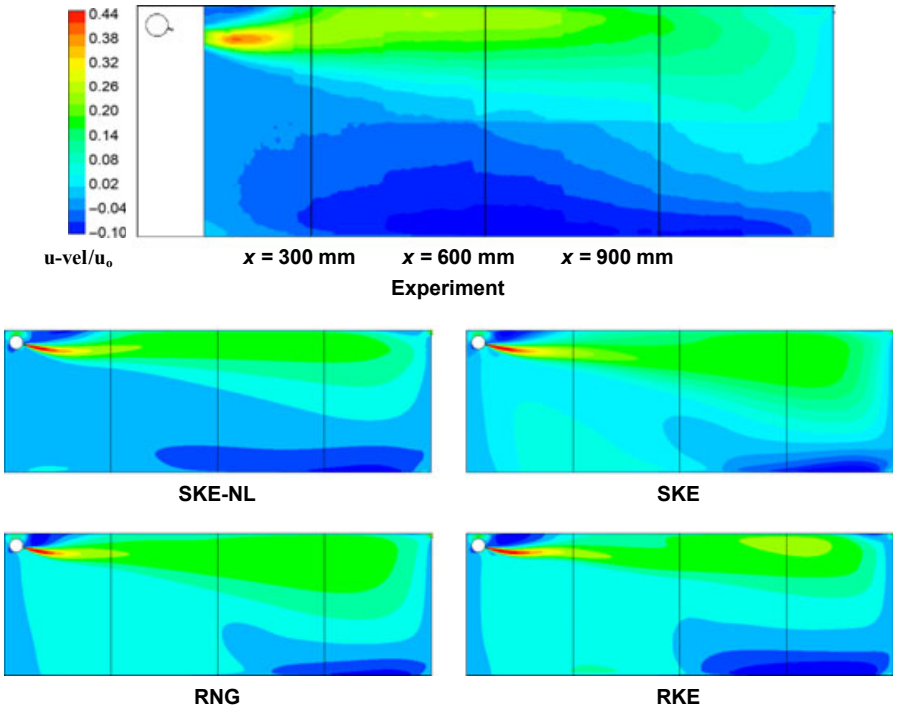

Fig. 6 Comparison of the u-velocity contours in the mid z-plane of Room-1. The measurement region is the complete cross-section

depicted in Figure 8 for three locations (x = 300 mm, 600 mm and 900 mm as depicted in Figure 6). The turbulence models are able to capture the peak velocities reasonably along the height at x = 300 mm. However, the reverse flow region below the jet flow is not captured at all by any of the linear k-ε models. The flow axial velocity remains positive; no recirculation is found. As the flow develops downstream, the linear models eventually produce the recirculation in the lower half of the room (x = 900 mm). The proposed

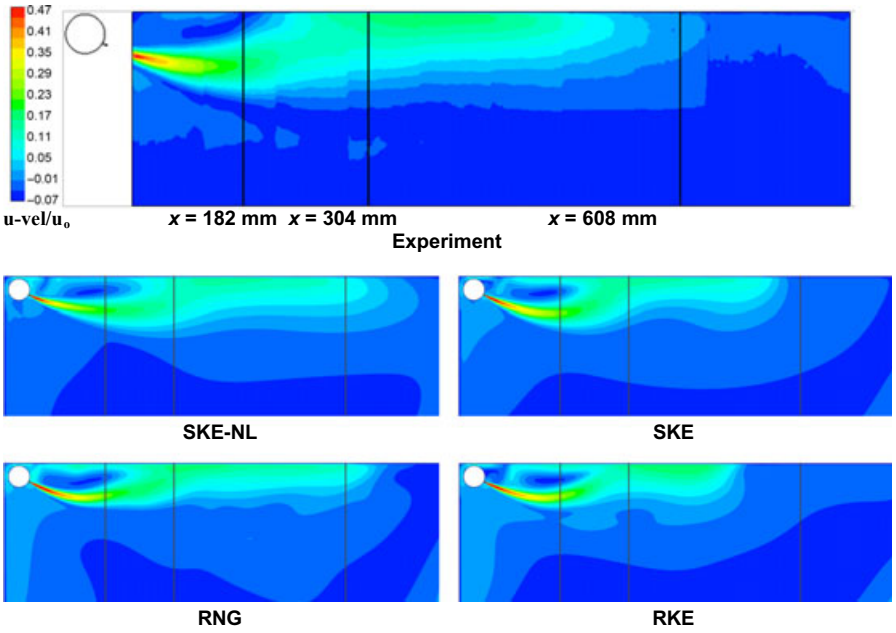

Fig. 7 Comparison of u-velocity contours in the mid z-plane for Room II. The measurement region shows a height of 195 mm from ceiling and the complete room length 883.1 mm

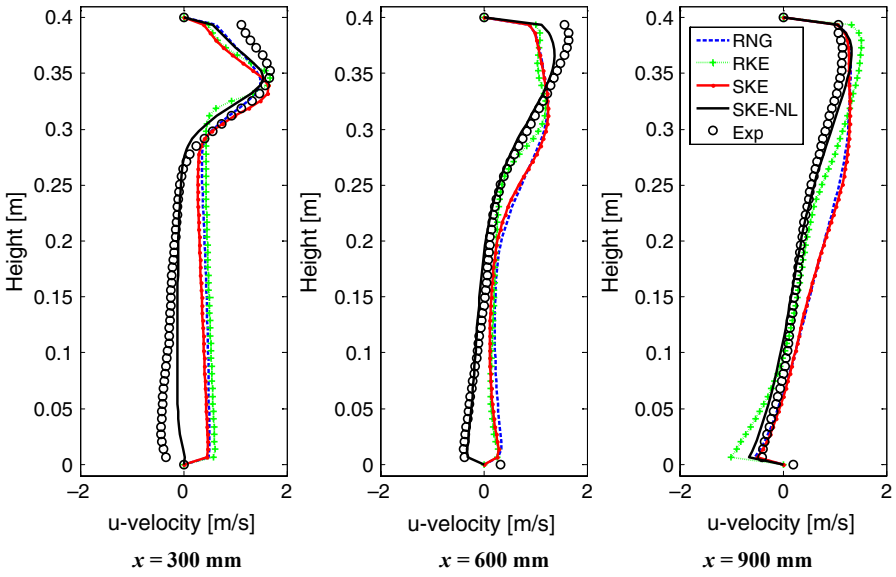

Fig. 8 Axial velocity (u-component) profiles in the vertical coordinate in the z-midplane (PIV measurement data determined with moving-average validation), taken at x = 300 mm, x = 600 mm, and x = 900 mm of Room-1

SKE-NL model shows significant improvements in capturing not only the recirculation but also the velocity profiles quantitatively. The improved prediction of the normal stress distribution by the nonlinear model enables the turbulence-driven secondary motion that enhances the prediction of the lateral spreading rate of the three-dimensional wall jet at the ceiling.

The turbulent kinetic energy (TKE) taken along the vertical lines x = 300 mm, 600 mm, and 900 mm are given in Figure 9 to highlight the differences in each of the k-ε-based turbulence models. The In the near inlet jet region the TKE profiles are similar for all models given that the flow development is not fully realized. Further downstream where the entrainment and turbulence-driven secondary motions become more influential, greater variation between the linear k-ε models with the nonlinear is much more evident. The nonlinear model provides has the ability to capture the secondary flow motions and turbulent normal stresses, whereas the linear models cannot.

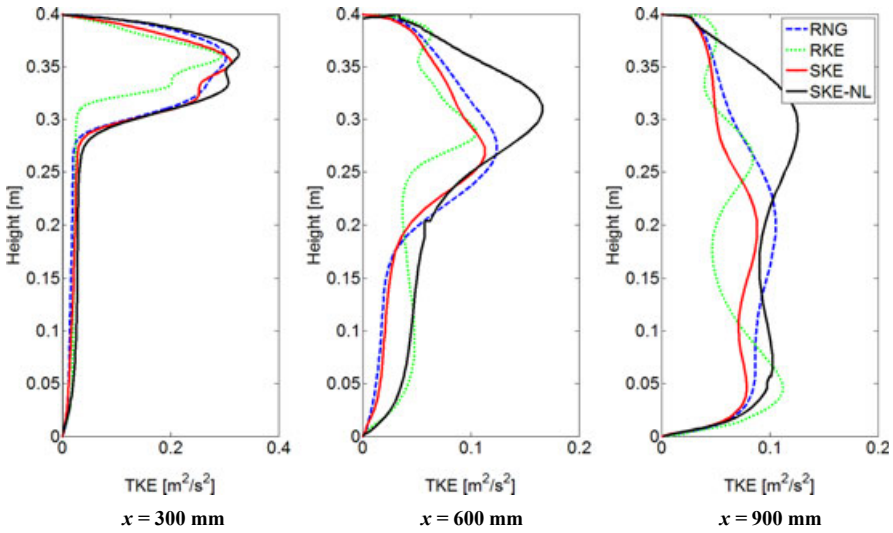

Fig. 9 Turbulent kinetic energy (TKE) profiles in the vertical coordinate in the z-midplane for Room-1 taken at x = 300 mm, x = 600 mm, and x = 900 mm of Room-1 as depicted in Figure 6

Conclusion

In industrial applications, RANS simulations with turbulence models are widely used. But generally, these models are not able to predict transitional effects, that is, the growing spreading rate of wall jets with lower Reynolds numbers. Especially at room airflows, often low inlet velocities prevail so that the transitional effect on the airflow pattern has to be considered. For this reason, a simple calibration procedure for eddy viscosity turbulence models which ensures the log-law and the correct shear layer behavior is presented. In addition, a nonlinear eddy viscosity model is suggested which reproduces the anisotropic Reynolds stresses and consequently turbulence-driven secondary motions. Finally, both approaches are validated with own experimental investigations of two different complex room airflows. Thereby, it could be shown that the proposed approaches can improve the prediction of linear jet diffuser flows.

Acknowledgements

The authors gratefully acknowledge the financial support provided by the Australian Research Council (project ID: DP120103958) and by the FFG structure program Josef Ressel-Zentrum 'CFD-Centre Austria'.

Supporting Information

Additional Supporting Information may be found in the online version of this article:

Figure S1. (a) Schematic of indoor flow phenomena caused by jet flows. (b) Definitions of lateral and normal spreading rates of jet flows. (c) PIV measurement planes.

References

Abrahamsson, H. (1997) *On Turbulent Wall Jets*, Göteburg Sweden, Chalmers University of Technology.

Chang, T.J., Hsieh, Y.F. and Kao, H.M. (2006) Numerical investigation of airflow pattern and particulate matter transport in naturally ventilated multi-room buildings, *Indoor Air*, **16**, 136–152.

Chen, Q. and Zhai, Z. (2004) The use of CFD tools for indoor environmental design. In: Malkawi, A. and Augenbroe, G. (eds) *Advanced Building Simulation*, New York, Spon Press, 119–140.

Coleman, H.W. and Steele, W.G. (1995) Engineering Application of Experimental Uncertainty Analysis, *AIAA J.*, **33**, 1888–1896.

Craft, T.J. and Launder, B.E. (2001) On the spreading mechanism of the three-dimensional turbulent wall jet, *J. Fluid Mech.*, **435**, 305–326.

Dantec (2002) *PIV Manual*, Skovlunde, Denmark, Dantec Dynamics A/S.

De Souza, F.A., Nguyen, D. and Tavoularis, S. (1995) The structure of highly sheared turbulence, *J. Fluid Mech.*, **303**, 155–167.

Demuren, A.O. and Rodi, W. (1984) Calculation of turbulence-driven secondary motion in non-circular ducts, *J. Fluid Mech.*, **140**, 189–222.

Deo, R.C., Nathan, G.J. and Mi, J. (2007) Comparison of turbulent jets issuing from rectangular nozzles with and without sidewalls, *Exp. Thermal Fluid Sci.*, **32**, 596–606.

Fluent (2007) *Fluent 12 User's Guide*, Centerra Resource Park, Lebanon, Fluent Inc.

Gatski, T.B. and Speziale, C.G. (1992) *On explicite algebraic stress models for complex turbulent flows. Technical Report* 92–58, Institute for Computer Application in Science and Engineering.

He, G., Yang, X. and Srebric, J. (2005) Removal of contaminants released from room surfaces by displacement and mixing ventilation: modeling and validation, *Indoor Air*, **15**, 367–380.

Heschl, C., Inthavong, K., Sanz, W. and Tu, J. (2013) Evaluation and improvements of RANS turbulence models for linear diffuser flows, *Comput. Fluids*, **71**, 272–282.

van Hooff, T., Blocken, B. and van Heijst, G.J. (2013) On the suitability of steady RANS CFD for forced mixing ventilation at transitional slot Reynolds numbers, *Indoor Air* **23**, 236–249.

Inthavong, K., Ge, Q.J., Li, X.D. and Tu, J.Y. (2012) Detailed predictions of particle aspiration affected by respiratory inhalation and airflow, *Atmos. Environ.*, **62**, 107–117.

Kim, J., Moin, P. and Moser, R. (1987) Turbulence statistics in fully developed channel flow at low Reynolds number, *J. Fluid Mech.*, **177**, 133–166.

Launder, B.E. and Spalding, D.B. (1974) The numerical computation of turbulent flows, *Comput. Methods Appl. Mech. Eng.*, **3**, 269–289.

Lübcke, H.M. and Th. Rung, F.T. (2003) Prediction of the spreading mechanism of 3D turbulent wall jets with explicit Reynolds-stress closure, *Int. J. Heat Fluid Flow*, **24**, 434–443.

Nielsen, P.V. (1990) Specification of a Two-Dimensional Test Case. *Book Specification of a Two-Dimensional Test Case*. Aalborg University, IEA Annex 20: Air Flow Patterns within Buildings.

Pope, S.B. (2000) *Turbulent Flows*, New York, Cambridge University Press.

Shih, T.H., Liou, W.W., Shabbir, A., Yang, Z. and Zhu, J. (1995) A new k-ε eddy viscosity model for high Reynolds number turbulent flows, *Comput. Fluids*, **24**, 227–238.

Sørensen, D.N. and Nielsen, P.V. (2003) Quality control of computational fluid dynamics in indoor environments, *Indoor Air*, **13**, 2–17.

Srebric, J. and Chen, Q. (2002) Simplified numerical models for complex air supply diffusers, *HVAC&R Res.*, **8**, 277–294.

Tavoularis, S. and Corrsin, S. (1981) Experiments in nearly homogenous turbulent shear flow with a uniform mean temperature gradient. Part 1, *J. Fluid Mech.*, **104**, 311–347.

Tavoularis, S. and Karnik, U. (1989) Further experiments on the evolution of turbulent stresses and scales in uniformly sheared turbulence, *J. Fluid Mech.*, **204**, 457–478.

Voigt, L.K. (2002) Validation of Turbulence Models using Topological Aspects, *Proceeding of ROOMVENT 2002*, 173–176.

Wilcox, D.C. (2006) *Turbulence Modeling for Cfd*, DCW Industries, Incorporated, La Canada, CA.

Yakhot, V. and Orszag, S.A. (1986) Renormalization group analysis of turbulence. I. Basic theory, *J. Sci. Comp.*, **1**, 3–51.

Zhai, Z.J., Zhang, Z., Zhang, W. and Chen, Q.Y. (2007) Evaluation of various turbulence models in predicting airflow and turbulence in enclosed environments by CFD: Part 1—Summary of prevalent turbulence models, *HVAC&R Res.*, **13**, 853–870.